Linear Recursive State Estimation of Hybrid and Unbalanced AC/DC Micro-Grids using Synchronized Measurements

Willem Lambrichts, *Student Member, IEEE,* Mario Paolone, *Fellow, IEEE,*

***Abstract*—In this paper, we present an exact (i.e. non-approximated) and linear measurement model for hybrid AC/DC micro-grids for recursive state estimation (SE). More specifically, an exact linear model of a voltage source converter (VSC) is proposed. It relies on the complex VSC modulation index to relate the quantities at the converters DC side to the phasors at the AC side. The VSC model is derived from a transformer-like representation and accounts for the VSC conduction and switching losses. In the case of three-phase unbalanced grids, the measurement model is extended using the symmetrical component decomposition where each sequence individually affects the DC quantities. Synchronized measurements are provided by phasor measurement units and DC measurement units in the DC system. To make the SE more resilient to vive step changes in the grid states, an adaptive Kalman Filter that uses an approximation of the prediction-error covariance estimation method is proposed. This approximation reduces the computational speed significantly with only a limited reduction in the SE performance. The hybrid SE is validated in an EMTP-RV time-domain simulation of the CIGRE AC benchmark micro-grid that is connected to a DC grid using 4 VSCs. Bad data detection and identification using the largest normalised residual is assessed with respect to such a system. Furthermore, the proposed method is compared with a non-linear weighted least squares SE in terms of accuracy and computational time.**

***Index Terms*—Linear state estimation, hybrid AC/DC grids, Kalman Filter, unbalanced networks, micro-grids.**

I. Introduction

HYBRID AC/DC grids are a promising solution to increase the share of distributed generation in future power grids that are expected to massively rely on renewable power generation. Indeed, combining AC and DC creates the opportunity for more flexible control and increased system's efficiency [1]. The knowledge of the system's state is a prerequisite for several key operational and control processes, such as grid-aware optimal power flow (OPF)-driven control [2], stability assessment, security and post-contingency analysis [3]. State estimation (SE) in solely AC grids, both static and recursive, is a well-understood problem where the literature has provided several solutions [4]. For hybrid AC/DC systems, instead, the SE still relies on different approximations as discussed in Section II.

The emerging availability of phasor measurement units (PMUs) provides synchronised measurements of the AC grid's current and voltage phasors at a rate of tens of frames-per-second [5]. Only when these phasors are written in Cartesian coordinates, the measurement model that relates the measurements to the states can be formulated in a strictly linear way. At the DC part of the system, DC measurement units (DMUs) may also provide synchronised measurements. The DC measurement model of a SE is intrinsically linear. The VSC model, however, linking the DC quantities to the complex AC phasors represented in Cartesian coordinates, does not intrinsically lead to a linear relationship between the states and the measurements. The VSC representation is, therefore, the key aspect in SE of AC/DC grids.

In this respect, this paper introduces a method to create a fully linear measurement model for VSCs using the complex modulation index of the VSC that links the real and imaginary parts of the complex phasors to the magnitude of the DC quantities. Using the symmetric component decomposition, the linear model is extended to unbalanced three-phase (3-ph) hybrid grids.

This paper proposes an exact recursive SE, relying on a Kalman Filter (KF) that uses a measurement model and the systems time evolution to estimate the unbiased and minimum variance states [3]. As known, the KF uses all available measurements, past and presents and it can be analytically proved that the estimation error of the KF is always lower than the estimation error of a static SE, provided that the KF process model hypotheses are correct [6]. The choice of the KF relies on the nature of the model we propose to take into account the converter's losses that, as a matter of fact, does require the previously computed state making the SE problem inherently recursive. Details and hypotheses about this aspect are described in the Appendix A. Furthermore, the SE is coupled with fast adaptive updates of the process model covariance matrix and is, therefore, highly suitable for step-varying states. Bad data in the AC and DC parts of the system are identified and rejected using the standard largest normalised residual (LNR) test.

The CIGRE benchmark 14 node AC micro-grid defined by Task Force C6.04.02 [7] is used to validate the SE. This benchmark grid is connected in 4 nodes to an 8 node DC grid using VSCs. The AC/DC hybrid grid is modelled and simulated in EMTP-RV, the electromagnetic transients program used to simulate the power system [8] [9]. Within the context of the European project HYPERRIDE under Grant agreement ID: 957788, the SE will be implemented into a real hybrid AC/DC micro-grid hosted at the Distributed Electrical System Laboratory at the EPFL. This real-life hybrid network

The authors are with the Swiss Federal Institute of Technology of Lausanne, 1015 Lausanne, Switzerland e-mail: (see willem.lambrichts@epfl.ch; mario.paolone@epfl.ch).

The project has received funding from the European Unions Horizon 2020 Research & Innovation Programme under grant agreement No. 957788.

requires updated state estimates in a fast (i.e. sub-second) and accurate way for different real-time grid-aware optimal control algorithms. The real systems topology and location of the PMUs and DMUs are identical to the ones used in the simulation for the validation of the state estimation.

The paper is structured as follows: Section II consists of a literature review on the SE of hybrid AC/DC networks, the transformer-like VSC model in the time domain and discusses the adaptive KF that uses the prediction-error covariance estimation method (PECE) to assess the process model error distribution. Section III presents the fully linear measurement model for lossless and lossy VSCs. Section IV describes the linear SE with bad data identification and an approximation of the PECE method. In Section V, the hybrid SE algorithm is validated in the EMTP-RV time simulation and its performance is compared with a non-linear weighted least square (WLS) SE. The conclusions are given in Section VI.

The technical contributions and innovations of this work include: 1) proposition of an exact and fully linear hybrid AC/DC network measurement model that includes the interfacing AC/DC converter losses; 2) proposition of a computationally-efficient approximation of the Kalman filter prediction-error covariance estimation (PECE) process proposed in [10]; 3) a recursive state estimator for hybrid AC/DC micro-grids capable to track system's state step changes including bad data detection and identification.

II. Literature Review

A. State estimation for hybrid AC/DC grids

The first applications of SE for hybrid AC/DC grids refer to HVDC lines and FACTS. Reference [11] describes a WLS SE for HVDC. A non-linear model of the VSC is used to link the AC system with the DC system using two relations: 1) the converter control inputs, namely the reference voltage magnitude and angle and 2) the power balance equations accounting for converter losses. [12] and [13] describe a solution for a linear SE for thyristor-based VSCs. Their solution exists in using the product of the voltage magnitude with the cosine of the firing angle and the excitation angle as state variables for the rectifier and inverter side. This approach makes the problem linear, however, its use is limited to only thyristor-based VSCs. Furthermore, this solution ignores converter losses. Other works incorporate the DC measurements using the non-linear power balance equations and use the modulation index as a measurement to link the DC voltage to the AC voltage magnitude [14]. [15] uses the power balance while ignoring the converter losses and iteratively solves the WLS SE using the partial derivative of the measurement equations.

When it comes to hybrid AC/DC grids with multiple DC links and an actual DC grid, fewer solutions have been proposed in the literature. [16] introduces a decentralised iterative technique that decomposes the SE problem of hybrid micro-grids. The authors suggest first to formulate the SE of the AC and DC part separately and subsequently, solve it alternated in an optimisation problem using the lossy active power balance to link the two systems. [17] and [18] follow a similar approach to solve the hybrid SE problem. [19] accurately models the conduction and switching losses of the AC/DC interfacing converter. However, this SE still relies on a non-linear VSC model. In [20], the authors propose a pseudo-dynamical hybrid model that can cope better with transient conditions that occur frequently on hybrid grids with VSCs. The formulated converter model is based on a lossless power balance equation and the modulation index, which defines the relations between the voltage magnitude at the AC side and the DC side. A more recent work [21] uses the same approach but includes the converter losses, formulated as a 2nd order polynomial, into the power balance.

All previously listed SEs make use of non-linear converter equations to describe the linkage between the AC and the DC state variables. This results in the need for a SE algorithm that uses an iterative procedure to find a solution. These iterative SEs are non-optimal and no unique solution can be guaranteed; [22] shows that using current magnitude measurements together with power flow measurements can cause the network to be not uniquely observable. Furthermore, suitable initial conditions need to be chosen to ensure convergence. Another problem in using an iterative algorithm is the computation time. SEs that run coupled with real-time control applications should find the optimal solution within time windows ranging from a few of hundreds of ms to a few seconds. Therefore, computational efficiency is crucial.

B. Adaptive Kalman Filter

Micro-grids are very often subjected to steps and fast state variations that violate the process model of recursive SE based on KF (see Appendix A). Therefore, a correct assessment of the prediction error covariance matrix $\tilde{\mathbf{P}}$ during these phenomena is crucial for the correctness of the KF. Various methods have been proposed in the literature to assess the process noise covariance matrix $\mathbf{Q}$ (e.g. [10], [23]–[26]). This work uses the prediction-error covariance estimation method (PECE), which is introduced in [10]. The PECE method only requires the setting of a single parameter and ensures the positive semi-definiteness of the estimated KF process covariance matrix (required to guarantee numerical stability). The method relies on the previous innovations as defined in (69) and computes an estimate of $\tilde{\mathbf{P}}_k$ without first making an estimation of the process noise covariance matrix $\mathbf{Q}_k$. The PECE method assumes the process model is an auto-regressive integrated moving average (ARIMA) (0,1,0) model [27], the system is fully observable and the measurement model is linear, fully known and time-invariant. The measurement covariance matrix $\mathbf{R}$ is assumed to be known. PECE considers that, when a step occurs, the KF state prediction (62) is inaccurate. Therefore, the absolute value of the innovations increases and the innovation covariance matrix approximation (1) changes. Consequently, the computed estimation covariance matrix $\tilde{\mathbf{P}}_k$ inflates and thus the Kalman gain too. Therefore, more weight will be put on the measurements model to instantly respond to the step change. To guarantee the positive definiteness of $\tilde{\mathbf{P}}_k$, a constraint convex optimisation problem based on ML estimation is solved (2).

The PECE is summarized here and all the details can be found in [10] and [28].

1) At time step k the a priori state estimate $\tilde{\mathbf{x}}_k$ is computed together with the innovation $\mathbf{y}_k = \mathbf{z} - \mathbf{H}_k\tilde{\mathbf{x}}_k$.
2) The covariance matrix of the innovations is given as:
$$\mathbf{S}_k = \mathbf{H}\tilde{\mathbf{P}}_k\mathbf{H}^T + \mathbf{R}_k \quad (1)$$
$\mathbf{S}_k$ can be approximated by $\hat{\mathbf{C}}_k = cov\left(\mathbf{y}_k, \mathbf{y}_{k-1}, \ldots, \mathbf{y}_{k-N+1}\right)$, with N the number of considered past innovations. In the static conditions, the sample covariance matrix $\hat{\mathbf{C}}_k$ tends to converge to the true $\mathbf{S}_k$ as N increases.
3) $\tilde{\mathbf{P}}_k$ can now be estimated. Because solving (1) to $\tilde{\mathbf{P}}_k$ will generally not produce a semi-definite matrix, a more adequate method has to be used: the authors of [10] suggest to solve the optimisation problem (2)
$$\begin{aligned} \min_{\mathcal{D}} \quad & \{-\log\left[\det(\mathcal{D})\right] + \text{trace}(\mathcal{D}\mathbf{E})\} \\ s.t. \quad & \mathcal{D} \text{ real symmetric, } \mathcal{D} \succ 0 \\ & I_n - \mathcal{D} \succcurlyeq 0 \end{aligned} \quad (2)$$
with
$$\mathbf{R}_k^{-1/2}\mathbf{H} = \mathbf{V}\begin{pmatrix}\mathbf{U}\\ \mathbf{0}_{m-n,n}\end{pmatrix} \quad (3)$$
$$\mathbf{E} = \left(\mathbf{V}^{-1}\mathbf{R}_k^{-1/2}\hat{\mathbf{C}}_k\mathbf{R}_k^{-1/2}\mathbf{V}^{-T}\right)_{(1:n,1:n)} \quad (4)$$
4) The optimisation problem (2) is solved with YALMIP using the *sdpt3* solver. The estimation for the prediction covariance matrix can subsequently be computed as:
$$\tilde{\mathbf{P}}_k = \left(\mathbf{U}^{-1}\left(\mathcal{D}^{-1} - I_n\right)\mathbf{U}^{-T}\right) \quad (5)$$

C. Transformer-like AC/DC converter model

A linear model of the converter is needed to link the AC phasors with the DC quantities. A transformer-like VSC model has been proposed in [29], [30]. Fig.1 shows the model of one inverter leg. The transformer-like model is derived from the power balance equations and allows to model the lossless behaviour but also the conduction losses and the switching losses separately. The modelling of the losses requires few parameters that can be derived from the component's datasheet. [31] further improved the transformer-like model accuracy by including the dead time and the high-impedance state. However, simulations show that the influence of these additional features is small and, therefore, they are not considered in this work.

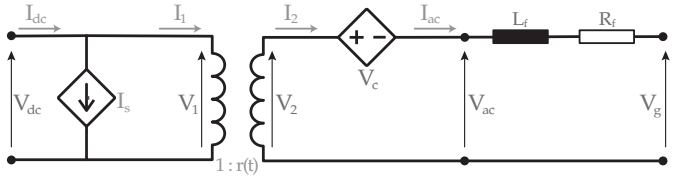

Fig. 1: Transformer-like model of an inverter leg of the AC/DC converter with RL filter

The lossless two-port time-domain model of an inverter leg can be derived as shown in (6), in which $r(t)$ is defined as the leg binary switching function between '0' and '1'. This variable, averaged over its switching period, is the same as the modulating function that gives the voltage reference to the converter legs.
$$\begin{bmatrix} v_2(t) \\ i_1(t) \end{bmatrix} = \begin{bmatrix} r(t) & 0 \\ 0 & -r(t) \end{bmatrix} \cdot \begin{bmatrix} v_1(t) \\ i_2(t) \end{bmatrix} \quad (6)$$
In the case of a lossy model, the conduction and switching losses can be included in the two-port model. The conduction losses account for the voltage drop over each conducting device. [30] suggests considering these losses as a voltage source in series with the transformer secondary side. The value of this voltage source depends on the direction of the alternating current and the switching function $s(t)$ that defines the conduction path. The **conduction loss** voltage drop in the time domain is represented by the difference between the ideal and the actual AC voltage (7) is analytically expressed as (8), in which V_T and V_D are the forward voltage drops over the transistor and the diode.
$$v_c(t) = V_{\text{DC}} r(t) - v_{\text{AC}} \quad (7)$$
$$v_c(t) = \text{sgn}(i_{\text{AC}}(t)) \left[\frac{V_T + V_D}{2}\right] + s(t)\frac{V_T - V_D}{2} \quad (8)$$
With $sgn()$ the sign function of the current in the time domain. The forward characteristics of the diode (referred to by subscript $_D$) and transistor (referred to by subscript $_T$) are approximated using a piecewise linear function with V_0 the forward voltage drop and R_0 the equivalent series resistance. Assuming the characteristics of the diode and the transistor hold, meaning $V_0 = V_{D0} = V_{T0}$ and $R_0 = R_{D0} = R_{T0}$, the conduction losses can be expressed as:
$$v_c(t) = V_0 \ \text{sgn}(i_{\text{AC}}(t)) + R_0 \ i_{\text{AC}}(t) \quad (9)$$
The **switching losses** are modelled as a current generator in parallel with the transformer primary side. Different methods have been proposed to model these losses [19], [29], [30], [32]. All methods are based on the transistor turn-on and turn-off losses under the test conditions:
$$E_{sw} = \frac{E_{ON} + E_{ON}}{V_{test} I_{test}} I_{ac} V_{dc} \quad (10)$$
The equivalent time commutation constants characterising the transistors turn-on and turn-off effects under the test conditions are defined as:
$$T_{ON} = \frac{E_{ON}}{V_{test} I_{test}}, \ T_{OFF} = \frac{E_{OFF}}{V_{test} I_{test}} \quad (11)$$
The switching losses are to a first approximation, proportional to the DC voltage and the instantaneous AC current. [29] [30] propose to model the current losses in the time domain for a fixed switching period as (12)
$$i_{s,IGBT}(t) = \frac{T_{ON} + T_{OFF}}{T_s} |i_{\text{AC}}(t)| \quad (12)$$
Other works, [19] and [32] propose to express the instantaneous energy losses due to the power semiconductor switching as (13).
$$E_{sw,IGBT} = (T_{ON} + T_{OFF}) V_{dc} \sqrt{2} I_{rms} \sin(2\pi f_{line} t), \quad (13)$$
where the current through the transistor is approximated as the fundamental line-frequency component of I_{ac}. Each time the

transistor switches, some energy is lost. Averaged over one grid period, the total switching energy is defined as (14):

$$E_{sw,IGBT,T} = 2(T_{ON} + T_{OFF})V_{dc}\sqrt{2}I_{rms}\sum_{n=1}^{N/2}\sin\frac{2\pi n}{N}, \quad (14)$$

with I_{rms} the rms value of the current, $N = \frac{f_s}{f_{line}}$, f_s the switching frequency and f_{line} the line frequency. Using trigonometric identities, the energy losses in (14) can be reformulated as a current in parallel with the transformer primary side:

$$I_{sw,IGBT,T} = 2\sqrt{2}\frac{T_{ON} + T_{OFF}}{T_s}\frac{1}{N}\cot(\frac{\pi}{N})I_{rms}. \quad (15)$$

The switching current losses for the diode are modelled in a similar way using the time constant T_{REC} representing the reverse recovery at turn-off (16).

$$I_{sw,Diode,T} = 2\sqrt{2}\frac{T_{REC}}{T_s}\frac{1}{N}\cot(\frac{\pi}{N})I_{rms}. \quad (16)$$

The total switching current losses are defined as the sum of (15) and (16)

III. Measurement Model of Hybrid AC/DC Networks

A. Converter Model

1) Lossless

Using the lossless transformer-like converter model Fig.1, the converter AC side can be linked with the DC side through the modulation index M. (17) describes the linkage for the lossless model, where $V_{ac} = V_2$ and $V_{dc} = V_1$ are the magnitudes of the AC and DC voltage.

$$V_2 = MV_1 \quad (17)$$

Because the AC system states are complex nodal voltages in Cartesian coordinates, (17) needs to be reformulated. By considering the modulation index as a complex variable $M = M_{re} + jM_{im}$, the problem can be reformulated so the DC quantities are linked with the AC phasors in a linear way:

$$V_{2,r} + jV_{2,i} = (M_{re} + jM_{im})\ V_1 \quad (18)$$

Because it is interesting to infer V_1 as a function of the complex phasors, we define:

$$M_{re}^{-} = \frac{M_{re}}{M_{re}^2 + M_{im}^2}, \quad M_{im}^{-} = -\frac{M_{im}}{M_{re}^2 + M_{im}^2}, \quad (19)$$

which leads to:

$$V_1 + j0 = (V_{2,re}M_{re}^{-} - V_{2,im}M_{im}^{-}) + j(V_{2,re}M_{im}^{-} + V_{2,im}M_{re}^{-}) \quad (20)$$

This reformulation leads to two linear relations that link the DC quantities to the AC complex phasors.

$$V_1 = V_{2,re}M_{re}^{-} - V_{2,im}M_{im}^{-} \quad (21)$$

$$0 = V_{2,re}M_{im}^{-} + V_{2,im}M_{re}^{-} \quad (22)$$

The current at the DC side can be analogously related to the AC current phasor:

$$I_1 = -(I_{2,re}M_{re} - I_{2,im}M_{im}) \quad (23)$$

2) Lossy

In the case of a lossy converter, the loss terms, defined in (9) and (15), need to be expressed using the phasor representation.

The **conduction losses** consists of two terms: an ohmic voltage drop proportional to the current and a constant voltage drop that changes sign depending on the current direction. The first term can straightforward be converted in phasor representation by taking the Fourier transform and only considering the fundamental frequency (24).

$$R_0\ i_{\text{AC}}(t) \xrightarrow{\mathfrak{F}} R_0 I_{AC,re} + jR_0 I_{AC,im} \quad (24)$$

The second term is a square wave with amplitude V_0. Using the Fourier expansion, the square wave can be represented by an infinite sum of sine waves. By neglecting the higher-order terms and taking the Fourier transform of the fundamental frequency, we can convert the time-domain expression into a phasor representation (25):

$$V_0\ \text{sgn}(i_{\text{AC}}(t)) \xrightarrow{\mathfrak{F}} V_0\frac{4}{\pi}\cos(\theta_I) + jV_0\frac{4}{\pi}\sin(\theta_I), \quad (25)$$

with θ_I the initial angle of the square wave function.

Using trigonometric identities, the voltage drop accounting for the conduction losses in an inverter leg can be written in phasor representation as:

$$\begin{aligned} V_{c,re} + jV_{c,im} =& (V_0\frac{4}{\pi}\cos(\theta_I) + R_0 I_{ac,re}) \\ &+ j(V_0\frac{4}{\pi}\sin(\theta_I) + R_0 I_{ac,im}) \\ =& (V_0\frac{4}{\pi}\frac{1}{|I_{\text{AC}}|} + R_0)(I_{ac,re} + jI_{ac,im}) \end{aligned} \quad (26)$$

The current magnitude in the denominator is computed using the states of the previous time step. The introduced approximation is negligible due to: 1) new states are computed at a very high frequency (i.e. lager than 1 Hz) and in quasi-static conditions, little difference will be observed between two consecutive states. 2) In recursive SE, the process noise can account for this error[1]. 3) The conduction voltage drop is at any time smaller than $0.005pu$. Therefore, even during large transients when the state would change abruptly between two consecutive time steps, the possible introduced error is very small. To represent the $V - I$ characteristic of the transistor with better accuracy, the real exponential relation can be used in preference to a linear piecewise function. Furthermore, the $R_{eq} - I$ characteristic, the ohmic resistance of the transistor as a function of its current can be derived from the semiconductor's datasheet. By using this characteristic, the value of the equivalent resistor R_{eq} is evaluated using the previously estimated state $|I_{ac}^{t-1}|$. Using R_{eq}, equation (26) is rewritten as (27).

$$V_{c,re} + jV_{c,im} = R_{eq}(|I_{ac}^{t-1}|)\ (I_{ac,re} + jI_{ac,im}). \quad (27)$$

The **switching losses** are also converted into Cartesian phasor representation. Both methods presented in Section II, (12) and (15) can be converter in a similar way by using the first-order Fourier expansion. It can be shown that both methods give the same numerical results.

$$\begin{aligned} I_{sw} = 2\frac{T_{ON} + T_{OFF} + T_{REC}}{T_s}\frac{1}{N}\cot(\frac{\pi}{N}) \\ \left(\cos(\theta_I^{t-1})I_{ac,re} + \sin(\theta_I^{t-1})I_{ac,im}\right) \end{aligned} \quad (28)$$

[1]The whiteness of this error is numerically proved in Section V-B

A **filter** at the AC side of the converter is required to reduce the harmonics to an acceptable level. Fig.1 shows the RL filter together with the lossy converter. The filter also needs to be included in the measurement model. We can write the voltage drop of the RL filter in phasor representation as:

$$\begin{aligned} V_{f,re} + jV_{f,im} =&(R_f + j\omega L_f)(I_{ac,re} + jI_{ac,im}) \\ =&(R_f I_{ac,re} - \omega L_f I_{ac,im}) + \\ & j(R_f I_{ac,im} + \omega L_f I_{ac,re}) \end{aligned} \quad (29)$$

Integrating the transistor losses (27) (28) and the filter voltage drop (29) into the lossless expression derived in (21), we get:

$$\begin{aligned} V_{\text{DC}} =&M_{re}^{-} \left(V_{g,r} + (R_f + R_{eq})I_{ac,r} - \omega L_f I_{ac,i}\right) \\ &- M_{im}^{-} \left(V_{g,i} + (R_f + R_{eq})I_{ac,i} + \omega L_f I_{ac,r}\right) \end{aligned} \quad (30)$$

and

$$I_{\text{DC}} = -\left(I_{ac,re}M_{re} - I_{ac_{im}}M_{im}\right) + I_s, \quad (31)$$

with I_s as defined in (28). The exact values of the complex modulation index can easily be extracted from the VSC control and will be fed to the SE as a known variable.

Because the states of AC systems are often selected as the nodal voltages, the DC voltage and current in (30) and (31) need to be rewritten as a function of the nodal AC voltages instead of the current flows. We call the nodes of the AC branch connected to the VSI k and m, with m the node closest to the VSC. Using the expressions (32), (33) of the real and imaginary part of the current flow phasors at the branch between buses k and m, we can formulate the VSC lossy model representing the DC voltage as a function of the AC nodal voltage phasors.

$$\begin{aligned} I_{km,re} =&g_{km,L}(V_{k,re} - V_{m,re}) - b_{km,L}(V_{k,im} - V_{m,im}) \\ &+ g_{km,T}V_{k,re} - b_{km,T}V_{k,im} \end{aligned} \quad (32)$$

$$\begin{aligned} I_{km,im} =&g_{km,L}(V_{k,im} - V_{m,im}) + b_{km,L}(V_{k,re} - V_{m,re}) \\ &+ g_{km,T}V_{k,im} + b_{km,T}V_{k,re} \end{aligned} \quad (33)$$

with $g = g_{km}$ the conductivity and $b = b_{km}$ the susceptibility of the line km. Rewriting (30) using the current flow equations with $I_{ac,re} = I_{km,re}$ and $I_{ac,im} = I_{km,im}$ gives for the direct sequence equivalent (1-ph):

$$\begin{aligned} V_{\text{DC}} =& \left[M_{re}^{-}\left(1 + (R_f + R_{eq})(g^L + g^T) - \omega L_f(b^L + b^T)\right)\right. \\ &+ M_{im}^{-}\left(\omega L_f(g^L + g^T) - (R_f + R_{eq})(b^L + b^T)\right)\left.\right]V_{m,re} \\ &+ \left[M_{re}^{-}\left(-(R_f + R_{eq})g^L + \omega L_f b^L\right)\right. \\ &+ M_{im}^{-}\left(-\omega L_f g^L + (R_f + R_{eq})b^L\right)\left.\right]V_{k,re} \\ &+ \left[M_{re}^{-}\left((R_f + R_{eq})(-b^L - b^T) - \omega L_f(g^L + g^T)\right)\right. \\ &+ M_{im}^{-}\left(1 + \omega L_f(-b^L - b^T) - (R_f + R_{eq})(g^L + g^T)\right)\left.\right]V_{m,im} \\ &+ \left[M_{re}^{-}\left((R_f + R_{eq})b^L + \omega L_f g^L\right)\right. \\ &+ M_{im}^{-}\left(\omega L_f b^L - (R_f + R_{eq})g^L\right)\left.\right]V_{k,im}, \end{aligned} \quad (34)$$

The coefficients $C_{1\ldots4}$ are introduced to simplify the above expression:

$$V_{\text{DC}} = C_1 V_{m,re} + C_2 V_{k,re} + C_3 V_{m,im} + C_4 V_{k,im}. \quad (35)$$

3) Unbalanced and 3-ph systems

In case of an AC 3-ph system, the measurement matrix is extended to included all the a, b, c-phases of the considered states and measurements. Therefore, the equations (30) and (31) need to be adapted in order to incorporate the 3-ph phasors, because one DC quantity needs to be related to three complex phasors. Using Fortescue's transformation to decompose the 3-ph voltages and currents into their symmetrical components, an elegant and linear solution is obtained. The complex linear transformation is shown in (36), where $\alpha = e^{\frac{2}{3}\pi j}$ and $0, 1, 2$ represents respectively the zero, positive and negative component.

$$\begin{bmatrix} V_{0_{re}} + jV_{0_{im}} \\ V_{1_{re}} + jV_{1_{im}} \\ V_{2_{re}} + jV_{2_{im}} \end{bmatrix} = \frac{1}{3}\begin{bmatrix} 1 & 1 & 1 \\ 1 & \alpha & \alpha^2 \\ 1 & \alpha^2 & \alpha \end{bmatrix} \cdot \begin{bmatrix} V_{a_{re}} + jV_{a_{im}} \\ V_{b_{re}} + jV_{b_{im}} \\ V_{c_{re}} + jV_{c_{im}} \end{bmatrix} \quad (36)$$

Using the symmetrical components decomposition, (21) is reformulated as (37) where each sequence contributes to the DC voltage.

$$\begin{aligned} V_{\text{DC}} =&M_{0,re}^{-}V_{0,re} + M_{1,re}^{-}V_{1,re} + M_{2,re}^{-}V_{2,re} \\ &- \left(M_{0,im}^{-}V_{0,im} + M_{1,im}^{-}V_{1,im} + M_{2,im}^{-}V_{2,im}\right) \end{aligned} \quad (37)$$

By solving (36) and substituting the real and imaginary components of the sequences into (37), a linear relation is obtained that links the DC voltage to the three complex phasors in the abc-coordinate system.

For a 3-ph system, the complex modulation indices M^{abc} are transformed into their symmetrical components M^{012} using the Fortescue matrix (36). The variables C_i in (35) become vectors consisting of $\left[C_i^0 C_i^1 C_i^2\right]^T$, for $i \in [1\ldots4]$. By re-transforming the variables into abc coordinates, the expression is obtained that links the DC voltage with the 3-ph AC phasors, this is directly used in the measurement model:

$$V_{\text{DC}} = \begin{bmatrix} \Re\left((C_1^{012} + jC_3^{012})^T A^{-1}\right) \\ \Re\left((C_2^{012} + jC_4^{012})^T A^{-1}\right) \\ \Im\left(-(C_1^{012} + jC_3^{012})^T A^{-1}\right) \\ \Im\left(-(C_2^{012} + jC_4^{012})^T A^{-1}\right) \end{bmatrix}^T \begin{bmatrix} V_{m,re}^{abc} \\ V_{k,re}^{abc} \\ V_{m,im}^{abc} \\ V_{k,im}^{abc} \end{bmatrix}, \quad (38)$$

with A^{-1} the inverse of the Fortescue matrix. The terms in (38) correspond to the submatrices $[\mathbf{H}_{VSC-AC}\ \mathbf{H}_{VSC-DC}]$ in the hybrid AC/DC measurement model (46) that will be constructed in the next section.

When VSC only injects the positive sequence component, the terms M_0 and M_2 in (37) can be omitted and the model simplifies. Therefore, the terms C_i^{012}, for $i \in [1...4]$ in (38) only have a positive sequence term: $[0\ C_i^1\ 0]^T$ and thus the DC voltage will only influence the positive sequence of the AC voltage.

It is important to notice that the proposed linear model allows for representing the VSC independently of its control variables and parameters. Because the SE is formulated from the grid's perspective, the internal voltages and/or currents within the VSC are not considered. The VSC control scheme regulates the modulation index to track the preferred set points for $V_{dc} - Q_{ac}$, $P_{ac} - Q_{ac}$ or $V_{dc} - |V_{ac}|$. Therefore, the states are estimated regardless of the control variables and the parameters.

B. AC Network Model

Using PMUs for the data acquisition allows formulating the AC system in a fully linear way. The measurements vector

consists of phase-to-ground nodal voltages, nodal current injections and current flows. In this work, the state variables, defined as the smallest set that fully describes the system, will be the nodal voltages for the AC network. The structure of the linear measurement model for the AC network is:

$$\mathbf{H}_{AC-AC} = \begin{bmatrix} \mathbf{H}_V & \mathbf{H}_{I_{inj}} & \mathbf{H}_{I_{flow}} \end{bmatrix}^T \tag{39}$$

The construction of these sub-matrices is described in [3].

C. DC Network Model

DMUs are responsible for the data acquisition in the DC network. The devices are time synchronised with the PMUs and have the same measurement frame rate. They provide nodal voltage, current injections and current flow measurements. Analog to the AC system, the expression of the current injections in node i connected to s nodes is:

$$I_i = \sum_{\ell=1}^{s} g_{i\ell} \left(V_i - V_\ell \right) \tag{40}$$

The expressions of the current flows at the branch between busses i and ℓ are:

$$I_{i\ell} = g_{i\ell} \left(V_i - V_\ell \right) \tag{41}$$

The structure of the measurement model for the DC network can be written as:

$$\mathbf{H}_{DC-DC} = \begin{bmatrix} \mathbf{H}_V & \mathbf{H}_{I_{inj}} & \mathbf{H}_{I_{flow}} \end{bmatrix}^T \tag{42}$$

The sub-matrices are defined as:

$$\mathbf{H}_V = [\, \boldsymbol{\alpha} \,], \qquad \text{where} \;\; \alpha_{i\ell} = \begin{cases} 1 & \text{if } i = \ell \\ 0 & \text{if } i \neq \ell \end{cases} \tag{43}$$

$$\mathbf{H}_{I_{inj}} = \mathbf{G}, \qquad \text{with} \;\; \mathbf{G} \text{ the conductivity matrix} \tag{44}$$

$$\mathbf{H}_{I_{flow}} = [\, \boldsymbol{\theta} \;\; \boldsymbol{\delta} \,], \qquad \text{where} \;\; \begin{cases} \theta_{i\ell} = g_{i\ell} \\ \delta_{i\ell} = -g_{i\ell}, \end{cases} \tag{45}$$

with $g_{i\ell}$ the element at the i, ℓ position in the DC network's conductivity matrix.

IV. Linear State Estimator of Hybrid AC/DC Networks

A. Measurement model

The measurement model (46) is constructed using the submatrices of the VSC model (38), AC grid (39) and DC grid (42) defined in the previous section.

$$\mathbf{H} = \begin{bmatrix} \mathbf{H}_{AC-AC} & \mathbf{0} \\ \mathbf{H}_{VSC-AC} & \mathbf{H}_{VSC-DC} \\ \mathbf{0} & \mathbf{H}_{DC-DC} \end{bmatrix} \tag{46}$$

Depending on the grid topology, location of the measurement devices and the preference of DC state variables, we can choose to use the VSC voltage (30) or the VSC current (31) model for the measurement matrix. In case the DC states are the nodal voltages, we can link the voltage measurement at the DC side of the VSC to the state variables using a one-on-one relation. Therefore, the measured DC current can be related to the states using the current model (31). If the DC currents are the preferred states, a similar reasoning is made.

Furthermore, the measurement model requires to satisfy several conditions to preserve linearity. 1) The AC measurements and states must be expressed in Cartesian coordinates, idem for the measurement noise. 2) The converter model requires the complex modulation index that is given as a known variable by the VSC. 3) To take the VSC losses into account, the current of the previous time step is evaluated to compute the equivalent ohmic resistance of the transistor and diode.

The measurement noise originates from two sources: 1) the noise coming from sensors and 2) inaccuracies introduced in the phasor extraction at the PMU level. Table I shows the phase displacement and ratio error for several accuracy classes of the voltage transformers according to [33]. Table II summarizes the noise level for different percentages of magnitude and phase displacement of the rated current [34]. Because of the faster dynamic behaviour in micro-grids, P class PMUs are preferred that are characterized by a fast response. The typical maximum errors of P class devices with a total vector error of 0.14% are given in Table III [35]. Following the hypothesis for the summation of uncorrelated normal distributions, the cumulative maximum errors of the sensors and the PMUs are computed by summing the corresponding magnitude error and phase errors. The cumulative standard deviation of the measurement noise is equal to one-third of the maximum errors.

TABLE I: Limits of ratio error and phase displacement of the voltage transformer.

IT class	ratio error (%)	phase displ. (mrad)
0.1	0.1	1.5
0.5	0.5	6
1	1	12

TABLE II: Limits of ratio error and phase displacement of the current transformer for different values of the rated current.

IT class	ratio error (%)				phase displ. (mrad)			
% of rated	5%	20%	100%	120%	5%	20%	100%	120%
0.1	0.4	0.2	0.1	0.1	4.5	2.4	1.5	1.5
0.5	1.5	0.75	0.5	0.5	27	13.5	9	9
1	3.0	1.5	1.0	1.0	54	27	18	18

TABLE III: Limits of magnitude and phase error of the P class PMU and DMU.

Device	accuracy (%)	mag. error (%)	phase error (rad)
PMU (AC)	0.14	0.1	10^{-3}
DMU (DC)	0.14	0.1	-

The PMU measurements are expressed in the Cartesian coordinate system. Therefore, the corresponding noise distributions in polar coordinates must also be transformed into rectangular coordinates as described in [3]. This coordinate transformation does not preserve the normality of the noise distribution. However, for small noise levels, as sensors of classes $0.1 - 1$, the effect is not noticeable and we can assume the noise in rectangular coordinates is normally distributed. The diagonal elements of the measurement noise matrix $\mathbf{R}$ are composed of the aforementioned variances.

B. Adaptive Kalman Filter

The PECE method, introduced in [10], relies on finding the solution of a determinant maximization (MAXDET) optimisation problem to infer the KF process noise covariance matrix. This problem, as given in (2), is time-consuming to

solve and requires specific software. However, by considering the optimisation variable $\mathcal{D}$ as a diagonal matrix, the problem can be significantly simplified to reduce the computation time. As the authors of [10] described, the off-diagonal elements increase the response time and improve the state-tracking capabilities. However, even without considering these elements, the performance of the AKF is still significantly better than the original DKF during step responses. Assuming $\mathcal{D}$ only has diagonal entries the MAXDET problem in (2) can be simplified to (47) by performing the mathematical transformations: 1) the logarithm of the determinant of a diagonal matrix can be rewritten as the sum of the logarithms of the individual diagonal elements. 2) The trace is reformulated as the inner product of the diagonal elements of the two matrices.

$$\min_{\mathcal{D}} \left\{ -\sum_{i=1}^{n} \log(\mathcal{D}_i) + \mathcal{D}\ \mathrm{diag}(\mathbf{E})^T \right\} \quad s.t.\ 0 < \mathcal{D} \leq 1 \tag{47}$$

with $\mathcal{D}$ a vector with as length the number of state variables. This is a simple optimisation problem that does not need any specific solver. This simplification hugely speeds up the problem so it can be used in a real-time application[2].

C. Bad Data Processing

After the estimation process, the presence of bad measurements is examined. Bad data that corrupts the measurements, originates from sensors (e.g. malfunctioning, biases and bad calibration) or telecommunication systems (e.g. noise and interference). The LNR test is used for the identification and elimination of these bad data. The test uses the measurement residuals (48) that are defined as the difference between the measurement and the reconstructed measurement computed using the state estimates [36] [4].

$$r_i = z_i - \mathbf{H}_i \hat{x}_i, \quad i = 1, \ldots, m \tag{48}$$

Using (65), the residuals are reformulated and its covariance matrix can be computed [37]:

$$\begin{aligned} z - \mathbf{H}\hat{x} &= z - \mathbf{H}(\tilde{x} + \mathbf{K}(z - \mathbf{H}\tilde{x})) \\ &= (\mathbf{I} - \mathbf{HK})(z - \mathbf{H}\tilde{x}) \end{aligned} \tag{49}$$

$$\begin{aligned} \mathrm{cov}(z - \mathbf{H}\hat{x}) &= (\mathbf{I} - \mathbf{HK})\ \mathrm{cov}(z - \mathbf{H}\tilde{x})\ (\mathbf{I} - \mathbf{HK}) \\ &= (\mathbf{I} - \mathbf{HK})\ \mathbf{S}\ (\mathbf{I} - \mathbf{HK}) \end{aligned} \tag{50}$$

with S the innovation covariance matrix as defined in (70). Using the definition of the Kalman gain (64), $(\mathbf{I} - \mathbf{HK})$ can be rewritten as $\mathbf{RS}^{-1}$.

$$\begin{aligned} \mathbf{T} = \mathrm{cov}(z - \mathbf{H}\hat{x}) &= (\mathbf{RS}^{-1})\mathbf{S}(\mathbf{RS}^{-1}) \\ &= \mathbf{RS}^{-1}\mathbf{R} \end{aligned} \tag{51}$$

Using (51), the normalised residuals are defined by (52), in which $\mathbf{T}_{ii}$ represents the i^{th} diagonal element of the residual covariance matrix.

$$r_i^N = \frac{|r_i|}{\sqrt{\mathbf{T}_{ii}}}, \quad i = 1, \ldots, m \tag{52}$$

If $r_k^N > c$, with k the index of the largest normalized residual, this measurement will be suspected as bad data. c is the user-defined identification threshold, set at for instance 4. In case a measurement is identified as bad data, this measurement is eliminated and the KF re-estimates the states using the reduced measurement matrix. The above process is repeated until all normalised residuals are smaller than the defined threshold.

[2]A numerical validation showed that the diagonal approximation reduces the CPU time from 11.5 ± 0.26 s to 58.7 ± 2.8 ms.

V. Numerical example

A. Network

The linear SE is validated in an EMTP-RV simulation of the CIGRE benchmark micro-grid extended with a DC grid. Fig.3 shows the hybrid grid's topology with the loads and the power sources. The AC micro-grid has a base voltage of $400\,\mathrm{V}$ and the DC grid $800\,\mathrm{V}$, the base power for both networks is $100\,\mathrm{kW}$. Bus $B01$ is the *slack bus* that is connected to the $20\,\mathrm{kV}$ medium voltage grid through a transformer. The table in Fig.3 indicates the simulation's boundary conditions. In order to consider a more realistic model, a dynamic power injection profile coming from photovoltaic power generation has been added to the AC node $B09$ and the DC node $B23$. The PV generation profile is shown in Fig.2 and has been measured on the EPFL campus. The system unbalance is created by injecting a total difference of $20\,\mathrm{kW}$ between the phases. The VSC's control variables are the DC voltage and the reactive power at the AC side setpoints.

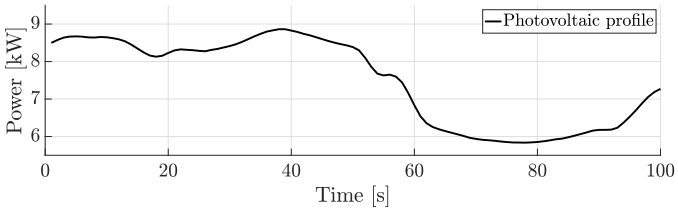

Fig. 2: Profile of the PV generation in nodes *B09* and *B23*

1) Measurements

The PMU and DMU locations are chosen to guarantee the observability of the system, i.e. the measurement model matrix $\mathbf{H}$ is full rank. On Fig.3, the PMU locations are shown in red and the DMU locations are in blue. Table IV summarizes the type of measurements that are provided for each bus.

The PMUs and DMUs provide measurements at 50 frames/s. The measurements are corrupted with white noise with a power spectral density identical to the noise of the PMU and the sensors used in the real system. The deployed current and voltage sensors for the AC and DC system have both an accuracy class of 0.5%. The measurement noise matrix is constructed using the corresponding sensors, PMU and DMU noise levels from Tables I, II and IV where the rated current of the sensors is chosen as the highest line ampacity in the network.

TABLE IV: PMU and DMU locations and measurement type in the Hybrid AC-DC micro-grid.

Network	Measurement type	Bus #
AC	3-ph Nodal voltage, 3-ph Current injections	1,3,5,9,11,13,14
AC	3-ph Current flows	9-15,13-16,11-17,7-18
DC	Nodal voltage	19,20,21,22,23,24,25,26
DC	Current flows	19-23,20-24,21-25,22-26

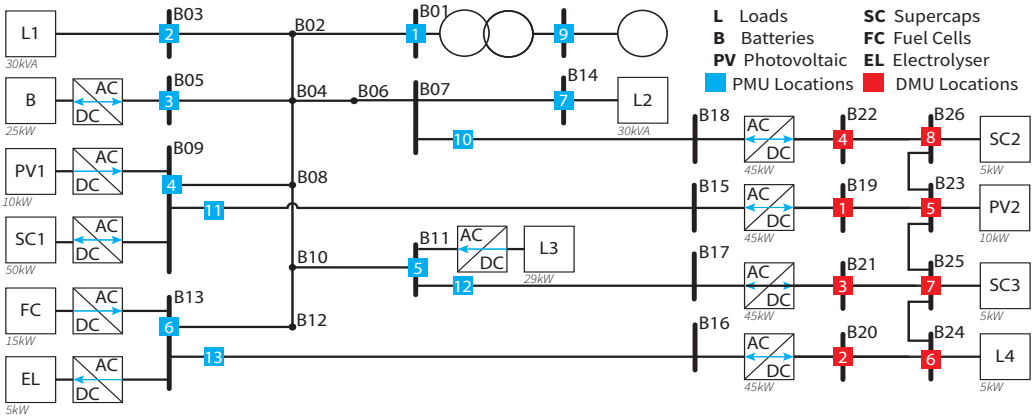

Parameter	Set point
L1	$-20\,\text{kW}, 0\,\text{var}$
B	$-20\,\text{kW}, -5\,\text{kvar}$
PV1	*Variable profile*
SC1	$2\,\text{kW}, 0\,\text{var}$
FC	$0\,\text{W}, 0\,\text{var}$
EL	$-10\,\text{kW}, 100\,\text{var}$
L2	$15\,\text{kW}, 300\,\text{var}$
PV2	*Variable profile*
SC2	$-5\,\text{kW}$
L3	$20\,\text{kW}, 2\,\text{kvar}$
SC3	$-5\,\text{kW}$
L4	$800\,\text{V}$
f	$50.0\,\text{Hz}$
V (B_{01})	$400\,\text{V}$

Fig. 3: Hybrid AC/DC micro-grid with the connected sources and loads, the maximum power rating are indicated. The table defines the boundary conditions of the simulation.

2) States

The state vector is composed of the nodal AC voltage phasors in rectangular coordinates and the current flows in the DC network:

$$\mathbf{x} = \left[V^{\ell}_{1,re}, \ldots, V^{\ell}_{k,re}, V^{\ell}_{1,im}, \ldots, V^{\ell}_{k,im}, I_{ij}, \ldots\right], \quad (53)$$

with ij the index of the DC current flows between busses $[19-23, 20-24, 21-25, 22-26]$, ℓ the phases a, b, c and k the index of the AC-side nodal voltage phasors at the busses 1 to 18 except for bus 6 and 12. These two busses are zero-injection busses that are removed from the SE using the Kron Reduction as described in [38]. Reducing the number of non-injection nodes is required to satisfy the observability criteria. Because the current is chosen as state for the DC system, the VSC voltage model (38) is used in the measurement model. For a 3-ph system, this results in 100 states and 120 measurements, meaning a redundancy factor of 1.2.

3) EMTP-RV time-domain simulation

The uncorrupted measurements and states of the network are obtained from an EMTP-RV time-domain simulation. The two-level converter is taken from the power electronics library and represents a detailed model of the power electronics switches and associated losses. The VSC is controlled using a control scheme that manages grid synchronisation under unbalanced conditions. In the simulation, the converters only inject the positive sequence currents. Therefore, correct detection of the voltage positive sequence components is essential. A double second-order generalized integrator (DGOSI) extracts the positive and negative sequence components of the grid voltage. The positive components are fed to a phase-locked loop (PLL) to extract the phase and the in quadrature dq voltage components in the rotating synchronous reference frame. The active and reactive power references, converted to dq current references using the in quadrature voltage components, are tracked using two coupled PI controllers with active saturation. The PI controllers are tuned using symmetrical optimum. A PWM signal at $5\,\text{kHz}$ controls the switching of the IGBTs. The AC and DC power sources, representing the different loads and sources are implemented in the time domain using a controlled current source. The converter and power sources are characterised by transient start-up phenomena that are ignored in the SE.

The AC measurement are generated using a discrete Fourier transform (DFT) that calculates the phasor quantities of the instantaneous values of the current and voltage signals. The phasors are calculated over a sliding window of one grid period equal. Because the time step of the simulation is 1 μs, 20000 samples are used the generate each phasors update. The measurements from the DMUs are generated similarly. However, instead of using a DFT to extract the phasor from the instantaneous signal, a moving average block has been used. The simulation model is made publicly available on the DESL GitHub page[3].

The process model is the ARIMA (0,1,0) to satisfy the PECE hypothesises.

B. Validation of the hybrid AC/DC state estimator

The validation of the hybrid SE relies on testing the assumptions made in (67) for the prediction error and (68) for the estimation error. If these expressions hold, the expected distribution equals the actual distribution and the hypothesis is valid. Therefore, the hybrid KF works properly and can be validated a posteriori (i.e. by means of the classical hypothesis verification process to assess the exactness of the SE model).

1) Validation of the estimation error

Fig.4 shows the fitted and expected distribution of the estimation error. The latter equals the square root of the diagonal elements of the estimation error covariance matrix $\hat{\mathbf{P}}$. The results are obtained for a $100\,\text{s}$ dynamic time-domain simulation of 5000 observations with respect to a system state associated with the boundary conditions given by the table in Fig.3. We can notice that the fitted distributions are zero biased and that their distributions are very similar to the expected distributions. Because of the readability of the figure, several AC state variables are omitted from the figure, however, these states exhibit the same behaviour. We can thus conclude that the hypothesis made in (68) is satisfied.

2) Validation of the prediction error

The actual and the expected prediction error distributions are shown in Fig.5. The expected distributions equal the square root of the diagonal elements of the prediction error covariance matrix. The fitted distribution has a zero mean and

[3]https://github.com/DESL-EPFL

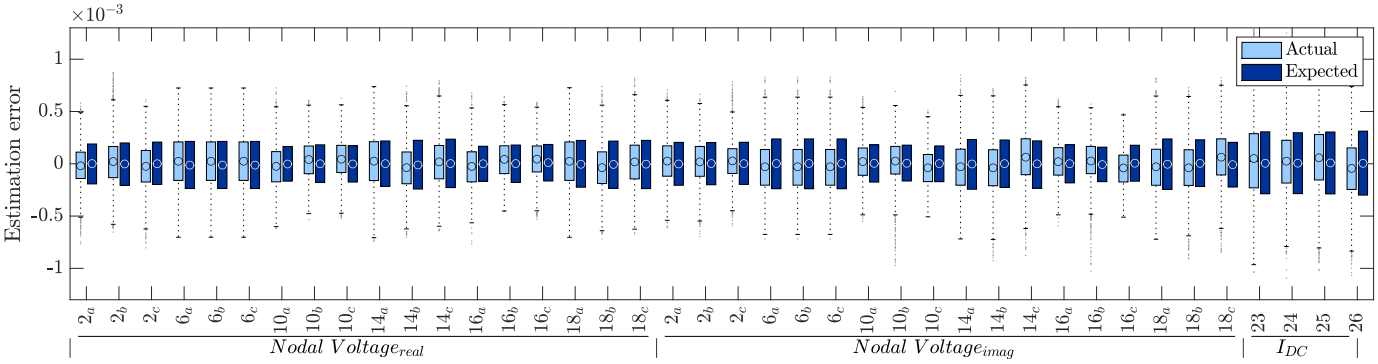

Fig. 4: Actual and expected distribution of the estimation error for the DC states and several of the 3-phase AC states.

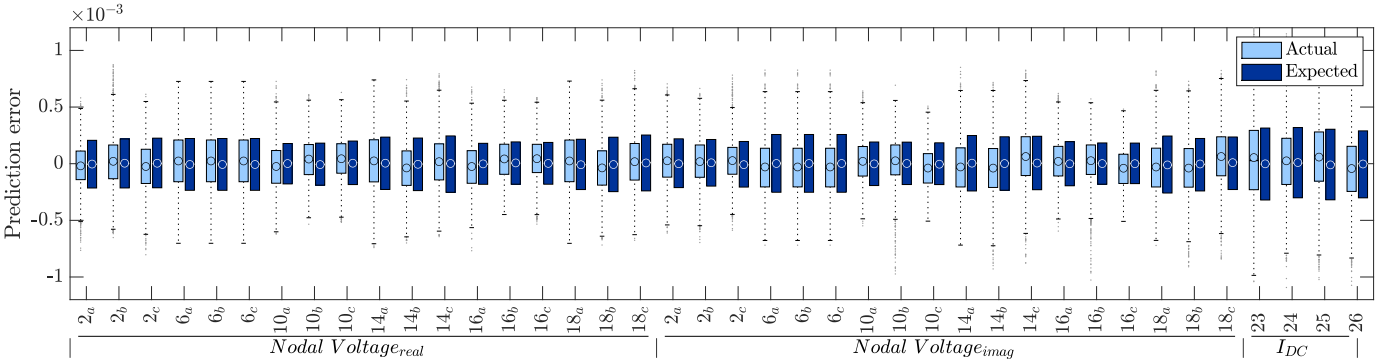

Fig. 5: Actual and expected distribution of the prediction error for the DC states and several of the 3-phase AC states.

its distribution is very similar to the expected one. The states that are not shown for the readability of the figure, exhibit the same behaviour. The hypothesis made in (67) can thus be validated.

3) Measurement model validation

The correct modelling of the linear VSC model in (37) is demonstrated on the residuals. The residuals of the DC voltage measurements define the difference between the measured DC voltage and the DC voltage reconstructed using the AC state estimates and the measurement matrix. When the distribution of the V_{dc} residuals is zero biased, the model is correct. Fig.6 shows the actual distribution of the residuals of the four DC voltages in busses *B19* to *B22*, namely the busses connected to the VSC DC side. The mean value is added to illustrate the residuals are unbiased and thus can be concluded that the VSC model is correct. Furthermore, is the expected distribution, defined in (51) highlighted on histograms to show the correct assessment of the residual covariance matrix. This implicitly shows the correctness of the LNR test as we will discuss in the next section on bad data detection and identification.

The influence of the loss terms on the accuracy of the SE is illustrated in Fig.7. The norm of the estimation error is shown for the two SEs: one with a measurement model that includes the loss term, and one with a model that ignores the VSC losses. Indeed, the inclusion of the loss term reduces the estimation error and therefore increases the accuracy of the estimated states.

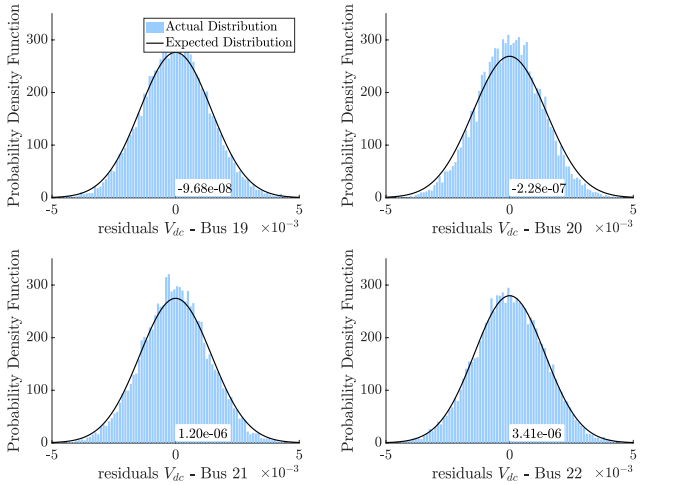

Fig. 6: Actual and expected distribution of the residuals of the DC voltage measurements in nodes 18,19,20,21

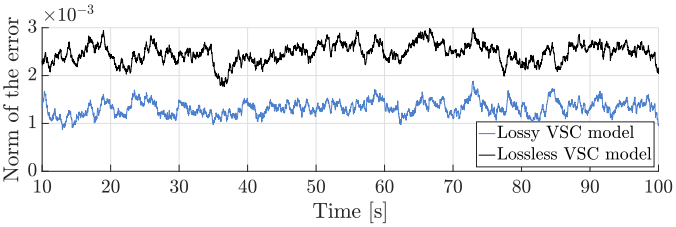

Fig. 7: Norm of the estimation error for the lossy and lossless VSC model. In the latter is not accounted for the switching and conduction losses.

C. PECE diagonal approximation

1) Validation of the PECE diagonal method

The approximation of the PECE method is validated by verifying the estimation error distributions (68). Fig.8 shows the actual and the expected distributions of the PECE and the PECE diagonal approximation method. Both methods are initialised by fixing the process noise to 10^{-6} for N time steps. The first 2 N time steps, N steps where the process noise is fixed and N time steps where the PECE is converging, are

removed from the simulation [10]. N is fixed at 2000 for both methods. The figure illustrates clearly the matching character of the distributions. The other state variables are omitted from the figure for readability, however, these states exhibit the same behaviour. We can thus conclude that the hypothesis is satisfied and the diagonal approximation is validated.

The dynamics of the DKF, the PECE and the PECE diagonal method are compared in Fig.9. After the initialisation time, a step in the injected power in node 7 is introduced and the response of the three methods is illustrated. The norm of the estimation errors clearly shows the large overshoot and the slow response of the DKF. PECE diagonal approximation has a larger overshoot than the PECE method but converges rapidly in less than $0.2\,\mathrm{s}$.

2) Influence of parameter N

Fig.10 shows the influence on the norm of the estimation errors (left) and the CPU time (right) for different values of N, the number of elements in the approximation of the innovation covariance matrix. The error bars define the 10^{th} and 90^{th} percentile of the computational time. The normalised error is computed considering a $100\,\mathrm{s}$ simulation for different values of N. The computation time is averaged over the simulation that is run on an Apple Macbook Pro laptop. The initialisation of the PECE method is the same as mentioned above. If N decreases, fewer samples are used in the estimation of the innovation covariance matrix and the measurement noise is less effectively filtered out. Therefore, the innovation covariance matrix is approximated less accurate and the norm of the estimation errors increases. Despite the lower accuracy, the dynamic response is faster for smaller N. This occurs because fewer samples are used and a step will have a larger influence on the innovation covariance matrix. The computational time slightly increases for increasing N, mainly because of the increasing complexity of the covariance matrix computation.

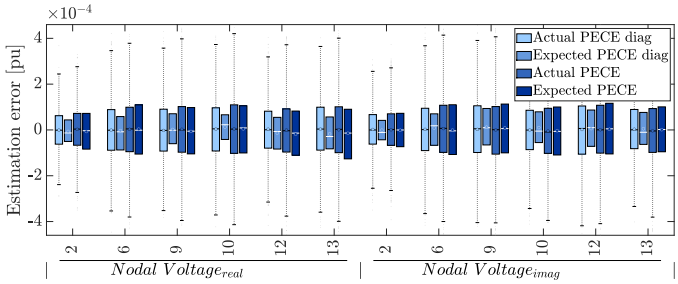

Fig. 8: Actual and expected distributions of the estimation error of the PECE method and the PECE diagonal approximation method

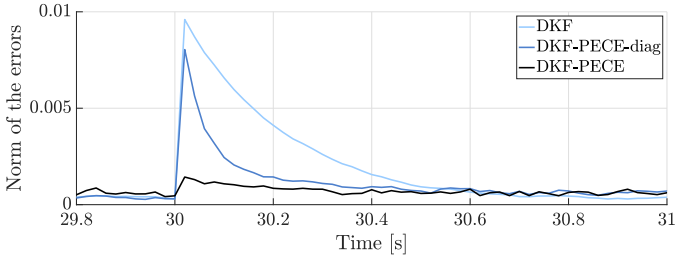

Fig. 9: Comparison of the dynamic response of the norm of the estimation errors between the DKF, PECE, and the PECE diagonal approximation method for N = 500.

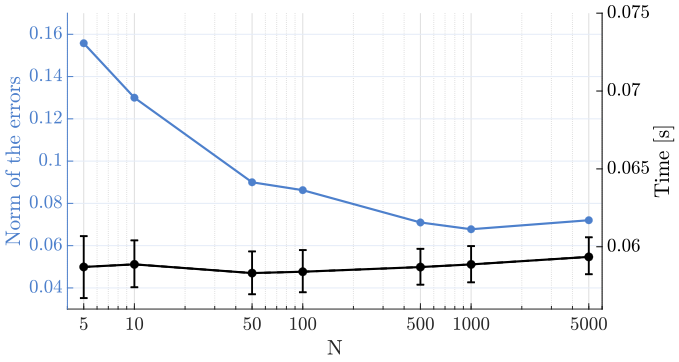

Fig. 10: Norm of the estimation errors and the corresponding computational time for different values of N in a $100\,\mathrm{s}$ simulation.

D. Bad data processing

The bad data identification and elimination capabilities of the LNR test are evaluated for the proposed SE. The LNR test identifies a measurement as erroneous when the normalised residual is larger than a predefined threshold. The optimal threshold, a compromise between the true positive and the true negative ratio is iteratively determined for the hybrid AC/DC grid. The true positive rate (TPR) is the ratio of the successfully detected bad data point over the total number of bad data points, while the true negative ratio (TNR) is the same for the non-erroneous measurement. Having two characteristics to evaluate the performance is crucial because a low threshold allows detecting many bad data points, but it could also misclassify correct measurements.

Erroneous measurements are systematically introduced in each of the measurement devices. 54 PMUs and 12 DMUs, defined in Table IV, measure the magnitude (and phase) of the AC and DC signals. For each measurement unit, a simulation is performed where several erroneous magnitude and phase measurements are introduced at random time steps. The erroneous measurement for measurement unit i at time step t is defined as $|z_i^t|(1+\alpha)$ with α a positive or negative value (50 % probability) and as absolute value a random sampled value between $(c, 5c] * \sigma_i$. The value c is the predefined threshold and σ_i is the measurement noise. Each simulation is $300\,\mathrm{s}$ and has 100 bad data points. Because of the transformation of the PMU measurements into rectangular coordinates, the erroneous measurement will propagate in both the real and imaginary parts. This will result in two coupled bad data points. The TPR and the TNR for bad data on the measurement magnitudes for a threshold of 4.5, are shown in Fig.11. This threshold is selected a posteriori. Since the value depends strongly on the system itself, an iterative process has been performed the find the threshold that exhibits the best bad data detection capabilities. The LNR test can successfully detect bad data in the large majority of the cases for both the AC and the DC system. Furthermore, the TNR shows that only a small fraction of the good measurements are incorrectly identified as bad data given this threshold. The measurements of the current injections in node B_{01} have a low TPR between 52% and 85%. These measurements exhibit the following characteristics: the currents are large, $1.3pu$, and the added noise is relatively small. Especially compared to the noise level of the states used to reconstruct this measurement. Therefore, the bad data,

which is proportional to the noise level will also be small and thus hard to detect. Bad data detection for phasor angles (not shown here due to space limitations) exhibits the same characteristics. The TPR is between 0.4 and 1 and the TNR is between 0.99 and 1.

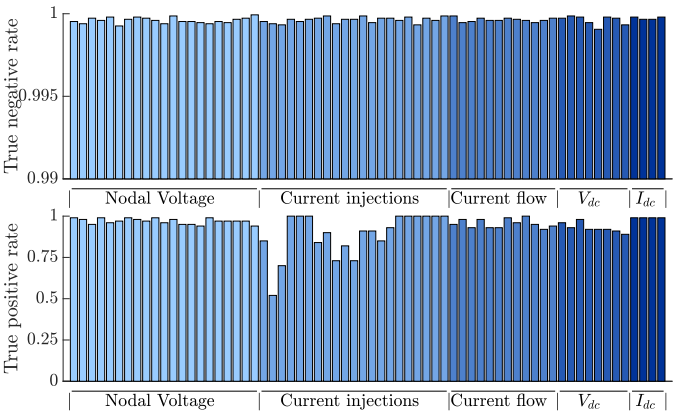

Fig. 11: True negative rate and the true positive rate of the LNR test.

E. Comparison with existing methods

The proposed linear recursive SE is benchmarked against existing methods from literature to assess its performance in terms of accuracy and computational time. A centralized non-linear WLS-based state estimation is used for the comparison [16]. For the correctness of assessment, the same simulation with the same voltage and current measurements is used as in the proposed SE.

The non-linear WLS is based on the widely adopted active power balance to relate the DC network to the AC network. The non-linear relation is included in the measurement model as a pseudo measurement, as defined in (54).

$$\mathbf{z}_{pseudo} = P_{AC}^{VSC} + P_{DC}^{VSC} + P_{loss}^{VSC} = 0, \tag{54}$$

The measurement vector is extended with the pseudo measurements as given in (55). The states $\mathbf{x}$ are chosen as the real and imaginary part of the AC voltages and the DC voltage magnitude (56).

$$\mathbf{z} = [\mathbf{z}_{AC}, \mathbf{z}_{DC}, \mathbf{z}_{pseudo}] \tag{55}$$

$$\mathbf{x} = [\mathbf{x}_{AC,re}, \mathbf{x}_{AC,im}, \mathbf{x}_{DC}] \tag{56}$$

Due to the non-linearity of the active power balance, the linearized measurement model needs to be expressed using the partial derivatives of the active power balance with respect to the state variables (57):

$$\mathbf{H} = \begin{bmatrix} \mathbf{H}_{AC,re} & \mathbf{H}_{AC,im} & \mathbf{0} \\ \mathbf{0} & \mathbf{0} & \mathbf{H}_{DC} \\ \dfrac{\partial \mathbf{z}_{pseudo}}{\partial \mathbf{x}_{AC,re}} & \dfrac{\partial \mathbf{z}_{pseudo}}{\partial \mathbf{x}_{AC,im}} & \dfrac{\partial \mathbf{z}_{pseudo}}{\partial \mathbf{x}_{DC}} \end{bmatrix} \tag{57}$$

The converter losses (58) are modelled similarly as in the proposed linear measurement model (27), following [31].

$$P_{loss}^{VSC} = (V_{c,re} I_{km,re} + V_{c,im} I_{km,im}) + I_{sw} V_{\text{dc}}, \tag{58}$$

with V_c the voltage drop due to conduction losses and I_{sw} the switching current losses. The loss term P_{loss} is written as a function of the state variables as shown in (59):

$$\begin{aligned} P_{loss}^{VSC} =& \left(\Delta V_{re}^2 + \Delta V_{im}^2\right)\left(g_L^2 + b_L^2\right)\Big(R_f + R_{eq}(|I_{ac}^{t-1}|)\Big) \\ &+ 2\frac{T_{ON} + T_{OFF} + T_{REC}}{T_s}\frac{1}{N}\cot\left(\frac{\pi}{N}\right)V_{\text{dc}} \cdot \\ &\Big[\Big(\cos(\theta_I^{t-1})g_L + \sin(\theta_I^{t-1})b_L\Big)\Delta V_{re} \\ &+ \Big(-\cos(\theta_I^{t-1})b_L + \sin(\theta_I^{t-1})g_T\Big)\Delta V_{im}\Big], \end{aligned} \tag{59}$$

where the grid parameters are the same as introduced in (32) and $\Delta V_{re} = (V_{k,re} - V_{m,re})$ and $\Delta V_{im} = (V_{k,im} - V_{m,im})$.

The comparison is made using the time-domain simulation as introduced in Section V. The measurement noise of the voltage and current measurements is identical as for the KF. For the sake of simplicity, the noise level of the pseudo measurements is set at 10^{-6}, i.e. an extremely low value that does not make the measurement covariance matrix ill-conditioned. The non-linear WLS is solved using an iterative Newton Raphson approach, with a tolerance of 10^{-5} and 10^{-6}. Table 12 summarizes the root mean squared errors (RMSE) of the state estimates and the computational time for the proposed method and the non-linear WLS. It can be seen that the accuracy of the estimated states of the proposed recursive SE is almost one order of magnitude better than the WLS one, with the CPU utilization time that is 5 to 10 times better. On average, it takes the WLS SE 15.1 iterations to reach the required tolerance of 10^{-5}; this explains the large improvement in computational time of the proposed SE.

The maximum estimation error at each time step is shown in Fig.12, where can be seen that the largest estimation error is a factor 10 smaller in the proposed method compared to the NL-WLS.

TABLE V: Accuracy and CPU time comparison between the DKF and the NL WLS.

	RMSE	CPU [ms]	Iterations
Non-linear WLS (10^{-6})	$1.812\ 10^{-2}$	27.4 ± 5.6	47.2
Non-linear WLS (10^{-5})	$1.836\ 10^{-2}$	12.2 ± 4.9	15.1
DKF (proposed method)	$1.386\ 10^{-3}$	2.86 ± 0.40	/

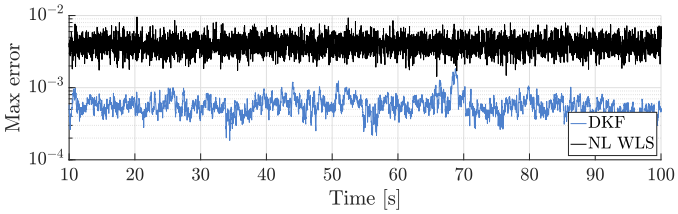

Fig. 12: Comparison of the maximum estimation error between the proposed DKF and the non-linear WLS SE.

VI. Conclusion

In this paper, it is introduced a fully linear measurement model for the recursive SE of hybrid AC/DC micro-grids. The measurement model includes a lossy VSC model that is based on the decomposition of the modulation index into its real and imaginary parts. The complex modulation index

can be directly obtained from the VSC controller. The model is further expanded for AC 3-ph unbalanced grids by using the symmetrical component decomposition. An EMTP-RV simulation of the CIGRE benchmark AC micro-grid connected using 4 VSCs to an 8 node DC micro-grid is used for the benchmarking of the hybrid SE. The SE and the measurement model are validated by verifying the hypotheses made on the prediction and the estimation error distributions. Furthermore, the influence of the lossy term of the VSC's model on the accuracy of the SE is illustrated. A comparison between the proposed SE and a non-linear WLS SE shows a major improvement in both CPU utilisation time and accuracy. The performance of the PECE diagonal approximation is shown and compared to the PECE method. The paper has also shown that, for the considered AC/DC grid and estimation frame rate, the required CPU time makes it suitable for control applications. Finally, the ability of the bad data detection and identification using the LNR test is verified for both AC and DC networks.

APPENDIX A
KALMAN FILTER

The Discrete KF relies on a measurement model and a process model [4]. The measurement model $\mathbf{H}$ relates the states variables $\mathbf{x}$ to the measurements $\mathbf{z}$. The measurement noise is assumed to be uncorrelated, unbiased, white and Gaussian with $\mathbf{R}$ the measurement noise covariance matrix. For the system to be observable, $\mathbf{H}$ needs to be full rank.

$$\mathbf{z}_k = \mathbf{H}\mathbf{x}_k + \boldsymbol{\epsilon}, \quad p(\boldsymbol{\epsilon}) \sim \mathcal{N}(0,\, \mathbf{R}) \tag{60}$$

The process model accounts for the time evolution of the system states. An ARIMA $(0, 1, 0)$ model [27] is used, which is very suitable for high-resolution measurements where the state between two consecutive time-steps does not change significantly. Because PMUs and DMUs are used that give newly updated synchrophasors every $20\,\mathrm{ms}$, this assumption is valid. The process noise is assumed to be uncorrelated, unbiased, white and Gaussian with $\mathbf{Q}_{k-1}$ the process noise covariance matrix.

$$\mathbf{x}_k = \mathbf{x}_{k-1} + \mathbf{w}_{k-1}, \quad p(\mathbf{w}_{k-1}) \sim \mathcal{N}(0,\, \mathbf{Q}_{k-1}) \tag{61}$$

Using (60) and (61), the linear KF equations are:

Prediction step:

$$\tilde{\mathbf{x}}_k = \hat{\mathbf{x}}_{k-1} \tag{62}$$

$$\tilde{\mathbf{P}}_k = \hat{\mathbf{P}}_{k-1} + \mathbf{Q}_{k-1} \tag{63}$$

Estimation step:

$$\mathbf{K}_k = \tilde{\mathbf{P}}_k \mathbf{H}^T (\mathbf{H}\tilde{\mathbf{P}}_k \mathbf{H}^T + \mathbf{R}_k)^{-1} \tag{64}$$

$$\hat{\mathbf{x}}_k = \tilde{\mathbf{x}}_k + \mathbf{K}_k(\mathbf{z}_k - \mathbf{H}\tilde{\mathbf{x}}_\mathbf{k}) \tag{65}$$

$$\hat{\mathbf{P}}_k = (\mathbf{I} - \mathbf{K}_k\mathbf{H})\tilde{\mathbf{P}}_k \tag{66}$$

$\mathbf{K}_k$ is the optimal Kalman gain, namely the value that minimizes the covariance of the estimation error, $\tilde{\mathbf{x}}_\mathbf{k}$ is the predicted state vector and $\hat{\mathbf{x}}_\mathbf{k}$ the estimated states. $\tilde{\mathbf{P}}_k$ and $\hat{\mathbf{P}}_k$ are the covariance matrices of the prediction and estimation errors and are defined as:

$$\tilde{\mathbf{P}}_k = \mathbb{E}[\tilde{\mathbf{e}}_k \tilde{\mathbf{e}}_k^T] \tag{67}$$

$$\hat{\mathbf{P}}_k = \mathbb{E}[\hat{\mathbf{e}}_k \hat{\mathbf{e}}_k^T], \tag{68}$$

with $\tilde{\mathbf{e}}_k = \mathbf{x}_k - \tilde{\mathbf{x}}_k$ and $\hat{\mathbf{e}}_k = \mathbf{x}_k - \hat{\mathbf{x}}_k$. $\mathbb{E}$ denotes the expected value. These relations are the hypothesis that are verified to validate the hybrid KF.

The innovation $\mathbf{y}_k$ (69) is defined as the difference between the measurement and the reconstructed measurements using the predicted state. Its covariance matrix is defined as (70).

$$\mathbf{y}_k = \mathbf{z}_k - \mathbf{H}\tilde{\mathbf{x}}_k \tag{69}$$

$$\mathbf{S}_k = \mathbf{H}\tilde{\mathbf{P}}_k\mathbf{H}^T + \mathbf{R}_k \tag{70}$$

REFERENCES

[1] N. Eghtedarpour and E. Farjah, "Power control and management in a hybrid ac/dc microgrid," *IEEE Transactions on Smart Grid*, vol. 5, no. 3, pp. 1494–1505, 2014.

[2] R. Gupta, F. Sossan, and M. Paolone, "Grid-aware distributed model predictive control of heterogeneous resources in a distribution network: Theory and experimental validation," *IEEE Transactions on Energy Conversion*, vol. 36, no. 2, pp. 1392–1402, 2020.

[3] M. Paolone, J.-Y. Le Boudec, S. Sarri, and L. Zanni, "Static and recursive pmu-based state estimation processes for transmission and distribution power grids," The Institution of Engineering and Technology-IET, Tech. Rep., 2015.

[4] A. Abur and A. G. Exposito, *Power system state estimation: theory and implementation*. CRC press, 2004.

[5] "Ieee standard for synchrophasor measurements for power systems," *IEEE Std C37.118.1-2011*, pp. 1–61, 2011.

[6] S. Sarri, L. Zanni, M. Popovic, J.-Y. Le Boudec, and M. Paolone, "Performance assessment of linear state estimators using synchrophasor measurements," *IEEE Transactions on Instrumentation and Measurement*, vol. 65, no. 3, pp. 535–548, 2016.

[7] S. Barsali, K. Strunz, and Z. Styczynski, "Cigre' task force c6.04.02: Developing benchmark models for integrating distributed energy resources," in *2006 IEEE Power Engineering Society General Meeting*, 2005.

[8] J. Mahseredjian, S. Lefebvre, and X. Do, "A new method for timedomain modelling of nonlinear circuits in large linear networks," in *Proc. of 11th Power Systems Computation Conference PSCC*, 1993.

[9] J. Mahseredjian, S. Dennetière, L. Dubé, B. Khodabakhchian, and L. Gérin-Lajoie, "On a new approach for the simulation of transients in power systems," *Electric power systems research*, vol. 77, no. 11, pp. 1514–1520, 2007.

[10] L. Zanni, J.-Y. Le Boudec, R. Cherkaoui, and M. Paolone, "A prediction-error covariance estimator for adaptive kalman filtering in step-varying processes: Application to power-system state estimation," *IEEE Transactions on Control Systems Technology*, vol. 25, no. 5, pp. 1683–1697, 2016.

[11] A. de la Villa Jaén, E. Acha, and A. G. Expósito, "Voltage source converter modeling for power system state estimation: Statcom and vsc-hvdc," *IEEE Transactions on Power Systems*, vol. 23, no. 4, pp. 1552–1559, 2008.

[12] W. Li and L. Vanfretti, "Inclusion of classic hvdc links in a pmu-based state estimator," in *2014 IEEE PES General Meeting| Conference & Exposition*. IEEE, 2014, pp. 1–5.

[13] H. Khazraj, F. F. da Silva, and C. L. Bak, "Modeling of hvdc in dynamic state estimation using unscented kalman filter method," in *2016 IEEE International Energy Conference*. IEEE, 2016, pp. 1–6.

[14] A. Mouco and A. Abur, "A robust state estimator for power systems with hvdc components," in *2017 North American Power Symposium (NAPS)*. IEEE, 2017, pp. 1–5.

[15] E. Zamora-Cárdenas, C. Fuerte-Esquivel, A. Pizano-Martinez, and H. Estrada-García, "Hybrid state estimator considering scada and synchronized phasor measurements in vsc-hvdc transmission links," *Electric Power Systems Research*, vol. 133, pp. 42–50, 2016.

[16] N. Xia, H. B. Gooi, S. Chen, and W. Hu, "Decentralized state estimation for hybrid ac/dc microgrids," *IEEE Systems Journal*, vol. 12, no. 1, pp. 434–443, 2016.

[17] X. Kong, Z. Yan, R. Guo, X. Xu, and C. Fang, "Three-stage distributed state estimation for ac-dc hybrid distribution network under mixed measurement environment," *IEEE Access*, vol. 6, pp. 39 027–39 036, 2018.

[18] L. Ping, K. Xiangrui, F. Chen, and Y. Zheng, "Novel distributed state estimation method for the ac-dc hybrid microgrid based on the lagrangian relaxation method," *The Journal of Engineering*, vol. 2019, no. 18, pp. 4932–4936, 2019.

[19] Z. Fang, Y. Lin, S. Song, C. Li, X. Lin, F. Wang, and Y. Lu, "A comprehensive framework for robust ac/dc grid state estimation against measurement and control input errors," *IEEE Transactions on Power Systems*, 2021.

[20] W. Li, L. Vanfretti, and J. H. Chow, "Pseudo-dynamic network modeling for pmu-based state estimation of hybrid ac/dc grids," *IEEE Access*, vol. 6, pp. 4006–4016, 2017.

[21] M. Ayiad, H. Leite, and H. Martins, "State estimation for hybrid vsc based hvdc/ac transmission networks," *Energies*, vol. 13, no. 18, p. 4932, 2020.

[22] A. Abur and A. Exposito, "Detecting multiple solutions in state estimation in the presence of current magnitude measurements," *IEEE Transactions on Power Systems*, vol. 12, no. 1, pp. 370–375, 1997.

[23] B. J. Odelson, M. R. Rajamani, and J. B. Rawlings, "A new autocovariance least-squares method for estimating noise covariances," *Automatica*, vol. 42, no. 2, pp. 303–308, 2006.

[24] L. Zanni, S. Sarri, M. Pignati, R. Cherkaoui, and M. Paolone, "Probabilistic assessment of the process-noise covariance matrix of discrete kalman filter state estimation of active distribution networks," in *2014 International Conference on Probabilistic Methods Applied to Power Systems (PMAPS)*. IEEE, 2014, pp. 1–6.

[25] G. Noriega and S. Pasupathy, "Adaptive estimation of noise covariance matrices in real-time preprocessing of geophysical data," *IEEE transactions on geoscience and remote sensing*, vol. 35, no. 5, pp. 1146–1159, 1997.

[26] K. Myers and B. Tapley, "Adaptive sequential estimation with unknown noise statistics," *IEEE Transactions on Automatic Control*, vol. 21, no. 4, pp. 520–523, 1976.

[27] A. S. Debs and R. E. Larson, "A dynamic estimator for tracking the state of a power system," *IEEE Transactions on Power Apparatus and Systems*, no. 7, pp. 1670–1678, 1970.

[28] L. Zanni, "Power-system state estimation based on pmus static and dynamic approaches - from theory to real implementation," Ph.D. dissertation, EPFL, Lausanne, 2017. [Online]. Available: http://infoscience.epfl.ch/record/228451

[29] A. Fratta and F. Scapino, "Modeling inverter losses for circuit simulation," in *2004 IEEE 35th Annual Power Electronics Specialists Conference*, vol. 6. IEEE, 2004, pp. 4479–4485.

[30] F. Scapino, "A transformer-like model for the dc/ac converter," in *IEEE International Conference on Industrial Technology, 2003*, vol. 1. IEEE, 2003, pp. 625–630.

[31] F. Scapino , "Vsi lossy models for circuit simulation including high-impedance state," in *Proceedings of the IEEE International Symposium on Industrial Electronics, 2005.*, vol. 2, 2005, pp. 565–570 vol. 2.

[32] Z. Fang, Y. Lin, S. Song, C. Li, X. Lin, and Y. Chen, "State estimation for situational awareness of active distribution system with photovoltaic power plants," *IEEE Transactions on Smart Grid*, vol. 12, no. 1, pp. 239–250, 2020.

[33] "Instrument transformers:, additional requirements for electronic current transformers,," Standard IEC, Tech. Rep. 61869-3, 2011.

[34] "Instrument transformers:, additional requirements for electronic current transformers,," Standard IEC, Tech. Rep. 61869-2, 2011.

[35] "Ieee standard for synchrophasor measurements for power systems," *IEEE Std C37.118.1-2011*, pp. 1–61, Dec 2011.

[36] T. Van Cutsem, M. Ribbens-Pavella, and L. Mili, "Hypothesis testing identification: A new method for bad data analysis in power system state estimation," *IEEE Transactions on Power Apparatus and Systems*, no. 11, pp. 3239–3252, 1984.

[37] J. Zhang, G. Welch, G. Bishop, and Z. Huang, "A two-stage kalman filter approach for robust and real-time power system state estimation," *IEEE Transactions on Sustainable Energy*, vol. 5, no. 2, pp. 629–636, 2013.

[38] A. M. Kettner, "Real-time state estimation and voltage stability assessment of power grids: From theoretical foundations to practical applications," Ph.D. dissertation, EPFL, 2019.

Willem Lambrichts received the B.Sc. degree in electrical engineering from the Catholic University of Leuven, Belgium in 2018 and the M.Sc in energy engineering from the Catholic University of Leuven in 2020. Since 2020, he is pursuing his Ph.D. degree at the Distributed Electrical Systems Laboratory, EPFL, Switzerland. His research interests include state estimation and optimal grid-aware control in the domain of hybrid AC/DC distributions networks.

Mario Paolone (M07, SM10, F22) received the M.Sc. (Hons.) and Ph.D. degrees in electrical engineering from the University of Bologna, Italy, in 1998 and 2002. In 2005, he was an Assistant Professor in power systems with the University of Bologna, where he was with the Power Systems Laboratory until 2011. Since 2011, he has been with the Swiss Federal Institute of Technology, Lausanne, Switzerland, where he is Full Professor and the Chair of the Distributed Electrical Systems Laboratory. His research interests focus on power systems with particular reference to real-time monitoring and operational aspects, power system protections, dynamics and transients. Dr. Paolones most significant contributions are in the field of PMU-based situational awareness of Active Distribution Networks (ADNs) and in the field of exact, convex and computationally-efficient methods for the optimal planning and operation of ADNs. Dr. Paolone was the founder Editor-in-Chief of the Elsevier journal Sustainable Energy, Grids and Networks.